EFDA–JET–CP(14)06/34

V.V. Plyusnin, C. Reux, V.G. Kiptily, A.E. Shevelev, J. Mlynar, M. Lehnen, P.C. de Vries, E.M. Khilkevitch, A. Huber, G. Sergienko, R.C. Pereira, D. Alves, B. Alper, U. Kruezi, S. Jachmich, A. Fernandes, M. Brix, V. Riccardo, L. Giacomelli, C. Sozzi, S. Gerasimov, A. Manzanares, E. de La Luna, A. Boboc, G.F. Matthews and JET EFDA contributors

Parameters of Runaway Electrons in JET

Parameters of Runaway Electrons in JET

V.V. Plyusnin[1], C. Reux[2], V.G. Kiptily[3], A.E. Shevelev[4], J. Mlynar[5], M. Lehnen[6], P.C. de Vries[6], E.M. Khilkevitch[4], A. Huber[7], G. Sergienko[7], R.C. Pereira[1], D. Alves[1], B. Alper[3], U. Kruezi[7], S. Jachmich[8], A. Fernandes[1], M. Brix[3], V. Riccardo[3], L. Giacomelli[9], C. Sozzi[10], S. Gerasimov[3], A. Manzanares[11], E. de La Luna[11], A. Boboc[3], G.F. Matthews[3] and JET EFDA contributors*

JET-EFDA, Culham Science Centre, OX14 3DB, Abingdon, UK

[1]Instituto de Plasmas e Fusão Nuclear, Instituto Superior Tecnico, Universidade de Lisboa, 1049-001 Lisboa, Portugal
[2]CEA, IRFM, F-13108 Saint-Paul-lez-Durance, France
[3]EURATOM-CCFE Fusion Association, Culham Science Centre, OX14 3DB, Abingdon, OXON, UK
[4]A.F. Ioffe Institute of the Russian Academy of Sciences, St Petersburg, 194021, Russia
[5]Association EURATOM/IPP.CR, IPP AS CR, CZ-18200 Prague, Czech Republic
[6]ITER Organization, Route de Vinon sur Verdon - CS 90 046 - 13067 St Paul Lez Durance, France
[7]Institute for Energy Research - Plasma Physics, Forschungszentrum Juelich, Association EURATOM-FZJ, Trilateral Euregio Cluster, 52425 Juelich, Germany
[8]Laboratoire de Physique des Plasmas- Laboratorium voor Plasmafysica, Association EURATOM-Belgian State, ERM/KMS, B-1000 Brussels, Belgium
[9]Department of Physics, Università degli Studi di Milano-Bicocca, Milano, Italy
[10]Istituto di Fisica del Plasma CNR-EURATOM, via Cozzi 53, 20125 Milano, Italy
[11]Association EURATOM-CIEMAT, Moncloa, Avd. Complutense, 22, 28040 Madrid 3, Spain
** See annex of F. Romanelli et al, "Overview of JET Results", (25th IAEA Fusion Energy Conference, St Petersburg, Russia (2014)).*

Preprint of Paper to be submitted for publication in Proceedings of the
25th IAEA Fusion Energy Conference, St Petersburg, Russia
13th October 2014 - 18th October 2014

ABSTRACT

The database on runaway electrons (RE) collected in JET with carbon-fibre composite tiles in plasma facing components (PFC) (JET-C) has been complemented by recent results of experiments on disruptions and RE generation in JET with full-metal ITER-like wall (JET-ILW). New experiments with Massive Gas Injection (MGI) provided conditions for predictable RE generation in disruptions. In these studies the RE generation process has been mapped in ranges on toroidal magnetic field, pre-disruption plasma density and fraction of argon used in mixture with deuterium (10÷100%) in MGI for future RE suppression experiments. New results on RE generation trends and disruption physics have been obtained. A significant extension of RE generation boundary to the lower magnetic fields (up to 1T) was found. RE current (up to 100kA) has been measured already at 1.2T. Temporal and spatial dynamics of RE beams have been studied using measured hard and soft X-rays emissions during RE stage. Energy spectra of RE have been measured. Data is used to contribute into the model of RE generation in the presence of spatial dynamics of current carrying channel and to the analysis of the interaction of RE beams with PFC.

1. INTRODUCTION

High-energy runaway electrons (RE) generated in major disruptions could cause severe melting of the Be-based plasma-facing components (PFC) in ITER. Therefore, an avoidance or suppression of RE generation is a task of high priority for ITER. Massive Gas Injection (MGI) from specially designed Disruption Mitigation Valve (DMV) is considered to be the most promising candidate method for suppression of RE generation and disruption mitigation [1]. In order to achieve the maximal efficiency of this method for RE beams dissipation a detailed knowledge of disruption evolution and RE generation physics is required.

In this paper the latest studies of RE generation process during disruptions in JET with fullmetal ITER-like wall (JET-ILW) are presented. The purpose of these experiments was to establish the ranges on toroidal magnetic field, pre-disruption plasma density and fraction of Argon (10÷100%) used in mixture with deuterium during MGI in order to achieve the predictable RE generation in disruptions for further experiments on RE suppression. The large database on RE generated at major disruptions in JET with carbon-fibre composite (CFC) tiles (JET-C) [2-4] has been used as reference for development of disruption scenarios for RE generation study in JET-ILW [5]. These experiments also provided sufficient data for comparison to JET-C results in order to clarify the influence of ITER-Like wall conditions on RE generation process.

2. DISRUPTION SCENARIOS AND RE GENERATION IN JET-ILW

To map the RE generation process at major disruptions in the space of JET-ILW operation parameters the triggering of disruptions by MGI with various D_2–Ar concentrations in their mixture was established as the best approach. A scan of Ar fraction in MGI was combined with variation of other operation parameters, such as toroidal magnetic field, plasma currents and initial pre-disruption plasma densities. Note, that accurate plasma density measurements during the early phase of the

current quench and RE generation were not available due to the interferometer laser refraction by density gradients in the post-thermal quench plasma. Therefore, initial plasma density values have been used as scan parameter. The L-mode target plasmas in divertor and limiter configurations were used for disruption scenarios development and mapping of RE generation process in JET parameters space. Plasma currents have been varied between 1.2 and 2MA in the range of magnetic field values $1T \leq B_0 \leq 3T$. Typical plasma parameters immediately preceding the MGI to trigger the disruptions were: electron density $10^{19} \leq ne \leq 4.5\times10^{19} m^{-3}$, and central electron temperature $T_e \sim$ 1.5÷3 keV. Figure 1 presents the most common features of the evolution of disruptions with MGI and RE generation in JET (JET Pulse No: 85978). DMV was triggered on 20.009 sec. Shortly after MGI (5÷10 msec) [1, 2] the JET plasma discharges due to increase of MHD activity entered into disruption stage with corresponding plasma thermal energy collapse, uncontrolled inward/vertical motions and, under certain conditions, RE generation observed as current plateaux and intense HXR and photo-neutron emissions. Detailed analysis of the evolution of parameters measured during MGI-triggered disruptions has demonstrated the following sequence of events. Approximately after 3÷6 msec from DMV trigger the toroidal set of fast MHD sensors (placed on the top of the JET vacuum vessel) registered the excitation of MHD perturbations with growing amplitude and propagating in the direction of electron flow (Figure 2). Excitation of regular or non-regular MHD perturbations has been detected also in MGI-triggered disruptions in last RE experiments in JET-C using MGI of pure Ar [2]. Duration of stages with described MHD activity revealed the dependence on Ar concentration in MGI: at larger concentrations this stage was shorter. Increment of these oscillations was much larger than those observed during slow gas injection from GIMs (in JET-C) before the fast stage of disruption [4]. Further growth of MHD activity resulted in onset of disruption fast (mixing) stage, which was terminated by complete plasma energy collapse (thermal quench, TQ) and reconnection of magnetic flux (highlighted by current bump and negative voltage spike). After this stage the disruption enters into current quench stage (CQ). Both types of disruptions – triggered by slow gas injection from GIM and by MGI (in JET-C and JET-ILW) – revealed the similarities in their dynamics during their fast (mixing) stages. First similarity concerns to impurity diffusion into plasma core and cooling processes. The SXR tomography carried out during TQ for both disruption types has shown the formation of hollow SXR emissivity profiles due to MHD-driven impurities transport to the plasma core and following core cooling (Figure 3). Bright emission islands (evidence for dominating m = 1 mode) have been observed in both types of disruptions. Measurements of electron temperature profiles using ECE radiometer also indicated the formation of hollow Te profiles immediately during current bumps in GIM-triggered disruptions [3, 4, 6] and for MGI case as well [6]. This fast (mixing) stage of disruptions resulted in well-understood plasma current re-distribution process which occurs following the changes in plasma conductivity profiles $\sigma(r,t)$ [7]. Analysis of current redistribution using induction equation:

$$r\frac{\partial E}{\partial r} = \frac{\mu_0}{2\pi}\frac{\partial}{\partial t}\left(\int_0^{a(t)} (\sigma(r,t)\cdot E(r,t))\cdot 2\pi r dr + \int_0^{a(t)} j_{RE}(r,t))\cdot 2\pi r\, dr\right)$$

indicates that during the mixing stage the formation of flat or even hollow current density profiles could be achieved.

During this process strong electric fields (up to E ~ 100V/m depending on difference between initial and final profiles) are induced inside the current inversion radius. Simplified analysis predicts that such values are high enough to enable RE generation (Dreicer), which together with hot-tail generation during fast plasma cooling creates the initial population of seed RE that is eventually amplified by secondary generation. In the same time range the plasma enters into current quench (CQ) stage. A scan on Ar fraction in MGI allowed establishing the boundaries for reliable and measurable RE generation starting from Ar concentrations of 40% in mixture with deuterium at the pressure of 33 bar in DMV (Figure 4). Conventional evaluation of RE current fractions generated during the CQ (assessment of deviation from exponential plasma current decay at simultaneous detection of HXR and photo-neutron yield) has demonstrated that RE could be generated in JET-ILW divertor configurations in a wide range of magnetic fields. Maximum RE current values achieved 350kA in disruption of discharge with ~1.9MA at B_0 = 3T (JET Pulse No: 85943). Reference disruptions triggered by MGI in limiter configurations resulted in generation of largest RE currents in JET-ILW. RE current plateaux higher than 1 MA with duration up to ~100 msec have been generated at injection of 100% argon and at different pressures in DMV. In JET-ILW as well as in JET-C the MGI-triggered disruptions in divertor configurations are characterized by higher plasma current time derivatives at the much lower generated RE populations in comparison to limiter configurations (Figure 5). In this figure it is also shown the crucial role of pre-disruption plasma density for RE generation. Generation of significantly lower RE currents were achieved at about 15÷20% of plasma density increase (green boxes). There was no substantial difference in RE generation when the second DMV (DMV-2) was spontaneously triggered in one pulse to provoke the disruption (Figure 5). However, another attempt to trigger the disruptions with DMV-2 installed close to equatorial plane of the torus was unsuccessful. This result requires an additional analysis. Location of the RE region in the JET-ILW parameters space (magnetic fields DMV pressure and argon fractions) was mapped where it was expected on the basis of data from JET-C runaway experiments [2, 3].

However, one of the important experimental result of these studies is the significant extension of the RE generation boundary towards to lower magnetic field values (Figure 6) – RE current up to 100kA was measured at magnetic field B = 1.2T, and measurable neutron yield has been detected even at B = 1T (RE current value was below the detecting level on plasma current exponential decay). Therefore, seemingly obvious threshold in magnetic fields for RE generation at major disruptions in tokamaks may in fact be the result of other factors and addressed rather to specific plasma parameters or technical features of devices. JET data reveals that the dependence of RE generation upper boundary on toroidal magnetic field is rather evolving proportionally to B2.

3. MEASUREMENTS OF RUNAWAY ELECTRON PARAMETERS

Relativistic RE interacting with background plasma, neutrals or surrounding PFCs produce a bremsstrahlung hard X-ray emission (HXR) in the MeV energy range and photo-neutrons.

Measurements of these radiations usually provide the information on energy characteristics of RE. For the device protection and RE studies 5 scintillation time-resolved HXR monitors and ^{235}U and ^{238}U fission chamber neutron rate monitors at 3 different locations operate in a current mode with 0.1ms time resolution [8]. The HXR emission has been measured with the set of horizontally and vertically viewing NaI(Tl), Bi_4GeO_{12} (usually referred as BGO) and $LaBr_3$ spectrometers. The data on spatial distribution of HXR emission sources in the plasma has been obtained with the JET neutron/gamma profile monitor routinely used for neutron and gamma rays measurements. The HXR raw data measured by BGO spectrometer has been processed with de-convolution procedure using the DeGaSum code [9]. This procedure allowed reconstruction of the energy spectra of generated RE populations. The RE distribution function (REDF) is important characteristic describing the RE generation process. Evolution of REDF can characterize different stages of this process such as acceleration of particles, their scattering on background plasma and neutrals, interaction with first wall, etc.

Reconstructed RE spectra revealed the larger maximal RE energies (up to 20MeV) in comparison to the maximal energies inferred from the HXR emission spectra and indicated the presence at several populations of RE electrons with different energies (Figure 6). The shape of reconstructed REDF appears to be different from that expected according to avalanche theory [10, 11]. Changes in shape of REDF with time during RE plateau stage (Figure 6) should be addressed to a combination of several different processes during CQ and RE plateau. In particular, the current substitution effect, when resistive current is substituted by RE current fraction thus decreasing the electric fields inside plasma column: $E_{||}(t) = E_{||0}(t)(1 - j_{RE}/(j_{pl} + j_{RE}))$, the dissipation of RE beams in surrounding plasma clouds containing high Z impurities from MGI (Ar, Ne, etc) and enhanced loss of high energy RE due to increased drift orbit shift. However, the reconstruction of REDF for different times during the RE plateaux does not allow direct answering how to separate the influence of current substitution effect and dissipation effects due to the presence of high-Z impurity gas cloud on RE energy spectrum. Yet another process, which inevitably should cause the change of REDF shape, is the interaction of RE beams with PFC. Numerical simulations of such interaction using Monte-Carlo code ENDEP [12] demonstrated that for certain combination of parameters of the incident RE (energy, pitch angle, etc.) their absorption could be less than the generation of additional secondary RE from the PFC surfaces [4]. In [5] it was reported that RE could pass the Be-tiles and return to the beam space with altered shape of energy spectrum. Obtained results definitely signify the necessity of certain improvement of the existing models for MGI and RE generation at disruptions and application of these models in numerical simulations. Analysis of REDF evolutions during RE plateaux (Figure 6) shows that RE populations with highest energies are lost in the first instance, while the populations with lower energies still exist on later stages of RE current plateaux and during their decay. This result well correspond to the fact that orbit shift of RE with increase of their energies will result in their loss. The decrease of effective plasma current-carrying channel due to current peeling effect (caused by plasma vertical and radial fast motions) is also affecting the confinement of RE with higher energies. Also the current peeling effect could sustain the flat or even hollow distributions

of RE currents during plateaux [13]. These issues were confirmed by HXR and SXR tomography reconstructions of RE beams and reported in [4].

3. EFFECT OF MGI ON RE PARAMETERS IN JET WITH ITER-LIKE WALL

Disruption monitor signals (photo-neutrons, HXR) have been used to study the characteristics of RE populations generated in JET disruptions. The loss of RE from confining region and their following interaction with PFC cause the HXR, SXR and photo-neutron emissions, which are consisting of steady state component and intense but short emission bursts. At the same time the decrease of RE plateau currents is usually measured. The termination of RE plateaux occurring as a sequence of current steps usually causes many intense HXR, SXR and photo-neutron bursts [11, 14]. A study of spatial evolution of RE beams and measured HXR, SXR, photo-neutrons and other parameters revealed the following: RE beams structure could consist of nested current-carrying toroidal shells with different current densities and energies of RE populations. In some cases the current densities in such toroids could achieve 1.5MA/m_2. Loss of such one thing toroidal layer (~40÷60kA) could cause the neutron yield comparable to total yield at the loss of 0.5 MA RE current plateau. However, very often the RE plateaux with up to 1MA current in JET-C have been terminated in one step resulting in intense, but in the one only burst of HXR and photo-neutrons. In this case the RE beam was consisting of one current-carrying channel, the loss of which terminated the whole plateau. Note, that the PFC materials in JET-C possessed the following photo-neutron bound energy εn thresholds: C – 18.7MeV, Ni – 12.0MeV, Cu – 10.6MeV, Ar – 9.9MeV. Energy of photoneutrons is $E_n = E_{HXR} - \varepsilon_n > 0$, therefore, the HXR energy and the energy of RE populations in JET-C is definitely higher than 10MeV and could achieve higher than E_{RE} ~20MeV [8, 4]. Also the photo-neutrons could be produced at interaction of RE and HXR with working gases and impurities. In JET-ILW the HXR energy should be higher than the neutron bound energy of the target nuclei: for deuterium – 2.2MeV, Be – 1.7MeV, W – 7.4MeV. Therefore, in JET-ILW we have lower thresholds for HXR and photo-neutrons measurements. Despite that after installation of ILW the lowered neutron yield energy thresholds for PFC materials (Be, W) do not allow direct quantitative comparison of the data measured in JET-C with data of JET-ILW, the analysis of trends in RE generation and interaction of RE with PFC and surrounding plasmas with high-Z impurities could be done. It is obvious that at larger densities and higher energies of RE interacting with PFC the flux of HXR and photo-neutrons will be higher, i.e. the higher signals will be measured (note that logarithmic scale of output signals). Usually the bursts of HXR and photo-neutron radiations constitute the dominating contribution into recorded parameters. Integrating the neutron signals from disruption monitors during the bursts times one can calculate the yield of photo-neutrons during the RE loss event (step-like plateau current decrease). Dependence of measured neutron yield versus values of generated (and/or lost) RE currents during one or several final loss events shows the increase of neutron yield for both – divertor and limiter configurations in JET-ILW (Figure 8a). HXR yield also increases with increase of RE currents. To get possibility for comparison of energetic characteristics of RE generated in different disruptions and different conditions we normalize the total yield of

photo-neutrons on values of RE current change. Total HXR yield caused by interaction of RE with impure plasmas also was used in analysis. The normalized HXR and neutron yields in MGI/divertor disruptions demonstrate the decreasing trends (Figures 8b and 8c (black circles)). Meanwhile the RE populations generated at MGI in limiter revealed at least non-decreasing trend (Figure 8c, blue boxes). Therefore, RE generated and lost at limiter configurations are more energetic since they produce more HXR and neutron emission events in comparison to cases of RE at MGI disruptions in divertor. More obvious effect of the presence of high-Z impurities in surrounding plasmas on energetic characteristics of RE populations could be deduced from the analysis and comparison of the data obtained in JET-C with both – MGI and GIMs scenarios, and JET-ILW with the use of MGI only.

Figure 9 presents the normalized neutron yield depending on values of RE current change at different disruption scenarios in JET-C – GIM (limiter) and MGI (limiter/divertor). The total number of injected argon atoms in GIM scenarios does not exceed $(2\div8)\times10^{20}$ particles. Meanwhile during MGI at a maximum pressure in DMV gas storage chamber up to 2.5×10^{23} particles could be injected. In MGI experiments [1, 2] the number of injected argon or neon (or their mixtures with deuterium) atoms has been varied between $(4\div6)\times10^{22}$ and $(21\div24)\times10^{22}$ [1-2, 4]. Therefore, the decrease of normalized neutron yield and, correspondently, the average energy of RE populations should be addressed to additional RE energy loss due to scattering on high-Z ions or due to enhanced collisional dissipation at higher electron density that also caused by high-Z impurity injection [15]. Figure 10 presents the effect of Ar fraction increase in MGI on normalized neutron yield in recent JET-ILW experiments. This figure also demonstrates the obvious dissipative effect on RE populations at increase of Ar fraction. However, the attempts to achieve the dissipation of existing RE beam plateau with the aid of direct MGI (using deuterium, argon or krypton) from the second DMV was hindered by poor penetration of the injected gas into the core of RE currentcarrying channel. It was observed that RE generation was successfully prevented if MGI was carried out in close time before the fast (mixing) stage of the disruption, while the 1.5 msec delay in MGI trigger didn't affect further generation of RE plateau with ~0.9MA.

4. SUMMARY

The mapping of RE generation domain in JET-ILW operation parameter space is carried out. The ranges on toroidal magnetic field, pre-disruption plasma density and the fraction of Argon (10÷100%) used in mixture with deuterium during MGI for the predictable RE generation at disruptions were established. Parameters of RE generated in JET with ILW have been measured. In JET-ILW the MGI-triggered disruptions in divertor configurations are characterized by higher plasma current time derivatives at lower generated RE currents in comparison to JET-C. The significant extension of the RE generation boundary towards to lower magnetic field values has been discovered. The RE current up to 100kA was measured at magnetic field B = 1.2T, and measurable neutron yield has been detected even at B = 1T (at very small RE current). Dissipative effects for RE populations caused by injection of high- Z impurity gas have been analysed. The decreasing trends in evolution

of RE energies with increase of injected gas quantity or with increase of Ar fraction in MGI were found. The first experiments on RE suppression using the MGI from the second DMV installed in JET-ILW have been carried out.

ACKNOWLEDGMENT

This work was supported by EURATOM and carried out within the framework of the European Fusion Development Agreement and of the Contract of Association between the EURATOM and Instituto Superior Tecnico and has also received financial support from Fundação para a Ciência e Tecnologia (FCT), Portugal. The views and opinions expressed herein do not necessarily reflect those of the European Commission or the ITER Organization. Also this work has been carried out within the framework of the EUROfusion Consortium and has received funding from the European Union's Horizon 2020 research and innovation programme under grant agreement number 633053. The views and opinions expressed herein do not necessarily reflect those of the European Commission.

REFERENCES

[1]. M. Lehnen et al, Nuclear Fusion **53** (2013) 093007;
[2]. V Riccardo et al, Plasma Physics and Controlled Fusion **52** (2010) 124018;
[3]. V.V. Plyusnin et al, Nuclear Fusion **46** (2006) 271;
[4]. V.V. Plyusnin et al, "Latest progress in studies of runaway electrons in JET" 24th IAEA FEC 2012, San Diego, USA
[5]. C. Reux et al, "Runaway beam studies during disruptions at JET-ILW" PSI2014;
[6]. S. Pestchanyi et al, Fusion Engineering and Design **88** (2013) 1127–1131
[7]. J.A. Wesson et al, Nuclear Fusion **30** (1990) 1011
[8]. O.N. Jarvis et al, Nuclear Fusion, **28** (1988) No.11
[9]. A. Shevelev et al, Nuclear Fusion **53** (2013) 123004
[10]. M. N. Rosenbluth and S. V. Putvinski, Nuclear Fusion **37** (1997) 1355
[11]. E.M. Hollmann et al, Nuclear Fusion **53** (2013) 083004
[12]. B. Bazylev et al. Journal of Nuclear Materials **415** (2011) S841–S844
[13]. S. Putvinski et al, Plasma Physics and Controlled Fusion **39** (1997) B157
[14]. R.D. Gill et al, Nuclear Fusion **42** (2002) 1039
[15]. K.O. Aleynikova et al. 40th EPS Conference on Plasma Physics (2013) O5.103

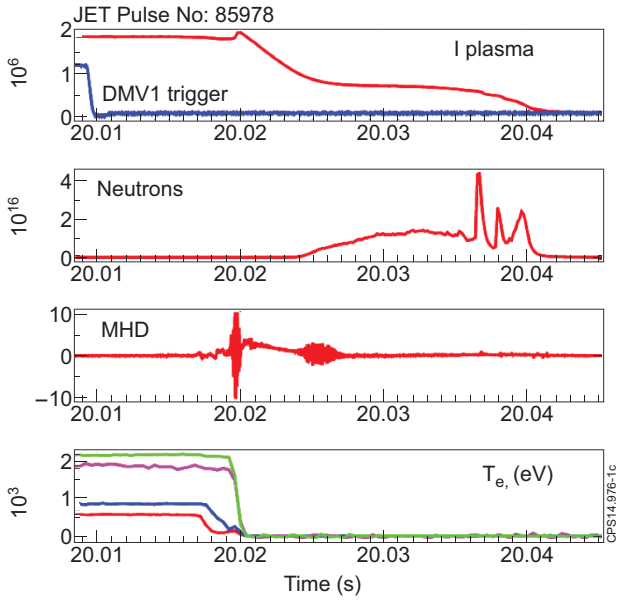

Figure 1: Time traces of disruption JET Pulse No: 85978 (MGI, 100% of Ar, DMV1).

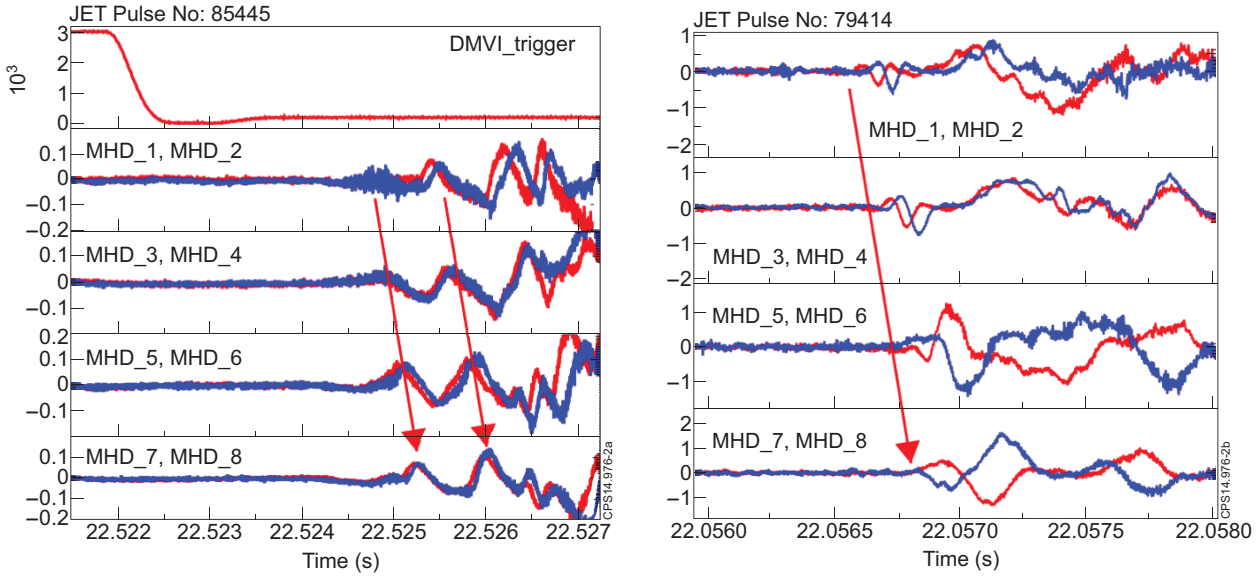

Figure 2: MHD activity in MGI-induced disruptions: Left chart – JET Pulse No: 85445, JET-ILW, divertor configuration; Right chart – JET Pulse No: 79414, JET-C, limiter, the DMV was triggered on t = 22.0484 sec (not shown); Each chart shows the signals from MHD sensors placed in each octant of JET from 1 to 8. Signals are plotted and numbered (1–2 (red & blue), 3–4, 5–6 and 7–8) according to counter-clockwise direction in JET plasmas – in the direction of electron flow.

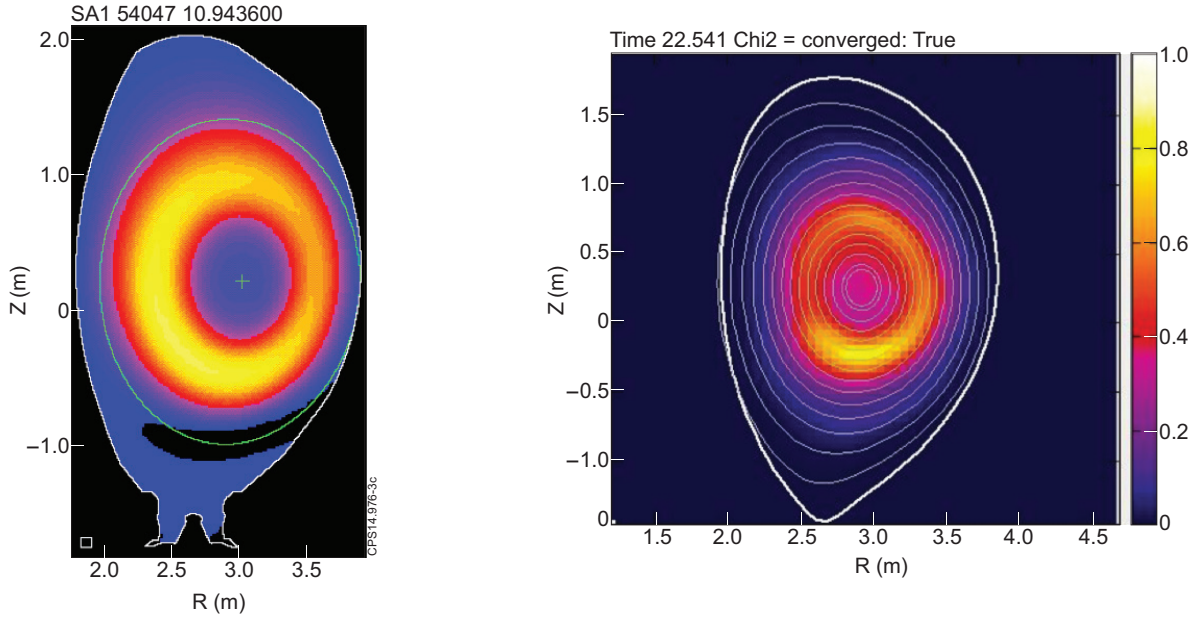

Figure 3: Comparison of SXR tomography during TQs in disruptions in JET-C (left chart, GIM, limiter) and JET-ILW (right chart, MGI, divertor). Reconstructions were performed at the beginning of current bump (fast disruption stage).

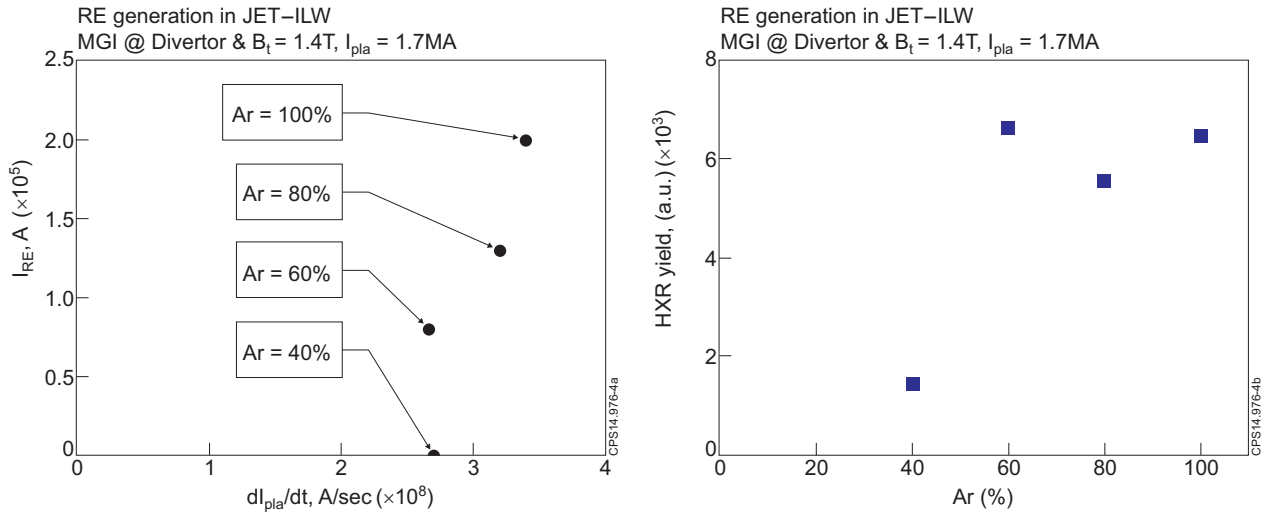

Figure 4: Scan on Ar fraction in MGI for disruption scenario development. Chart a: generation of RE currents versus plasma current time derivatives and chart b: HXR yield versus Ar fraction in MGI.

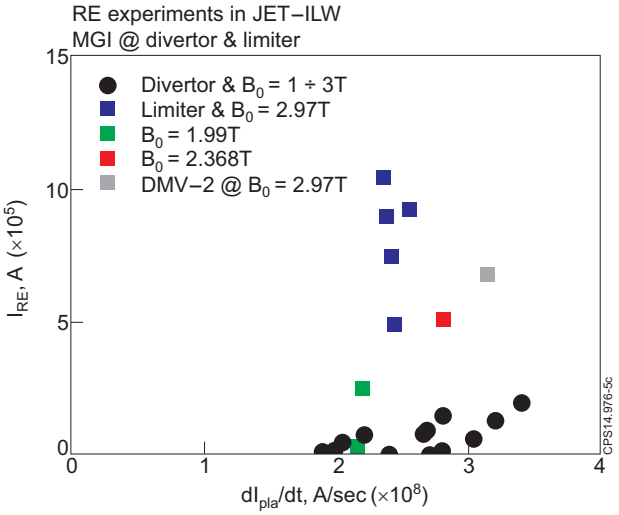

Figure 5: RE generation in divertor (circles) and limiter (boxes) configurations in JET-ILW. Effect of the lower initial plasma density on RE generation is presented by data shown as green boxes (higher RE current at lower density).

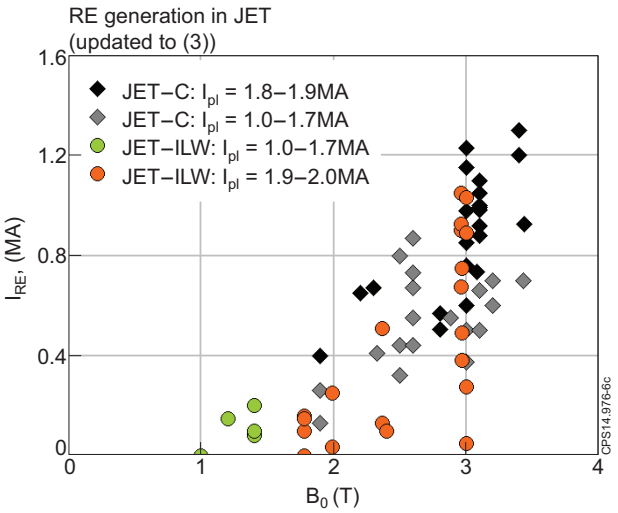

Figure 6: RE generation space in JET-ILW and JET-C vs. toroidal magnetic field value B0. The data collected in JET–C (diamonds, from [3]) is updated by recent results in JETILW (circles).

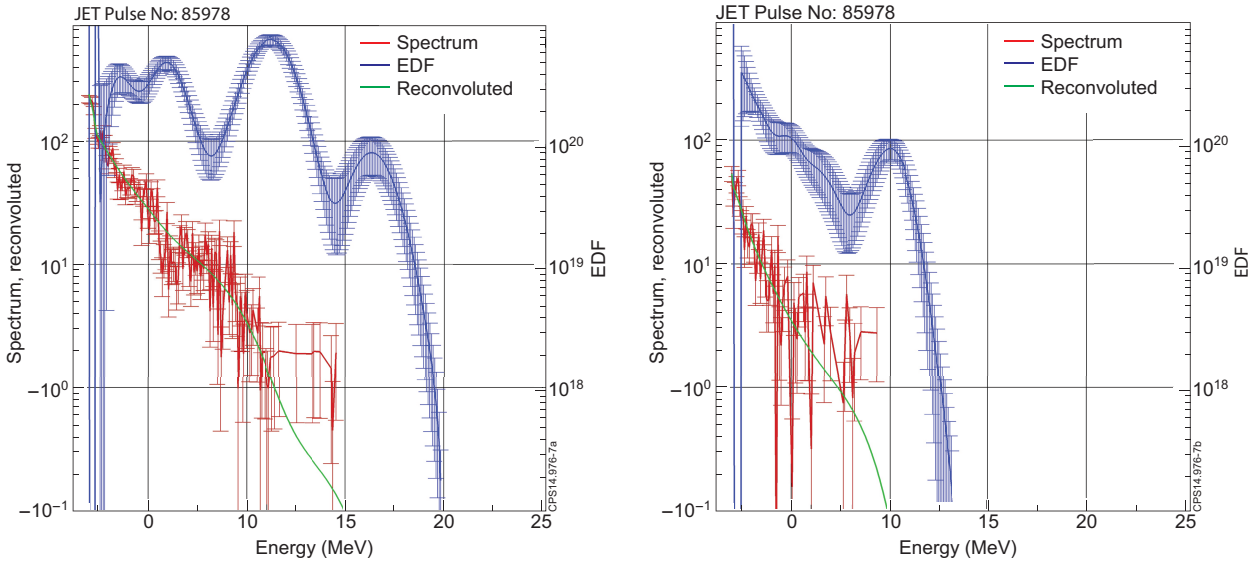

Figure 7: JET Pulse No: 85978: HXR spectra and Runaway Electron Distribution Functions (REDF) at the beginning of RE current plateau (t = 20.024-20.035 s, left chart) and at the end of RE plateau (t = 20.035-20.045, right chart). Measured HXR spectra (in red), compared to the spectra (in green) inferred from reconstructed REDF (in blue).

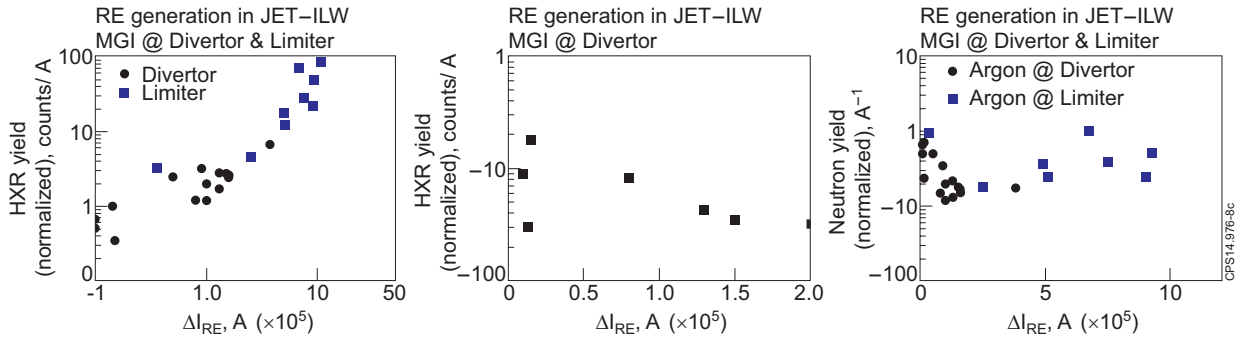

Figure 8: chart a – Total neutron yield versus RE currents, chart b – normalized HXR yield versus RE currents at MGI with Argon in divertor configuration; chart c – comparison of normalized neutron yields for divertor and limiter configurations at MGI.

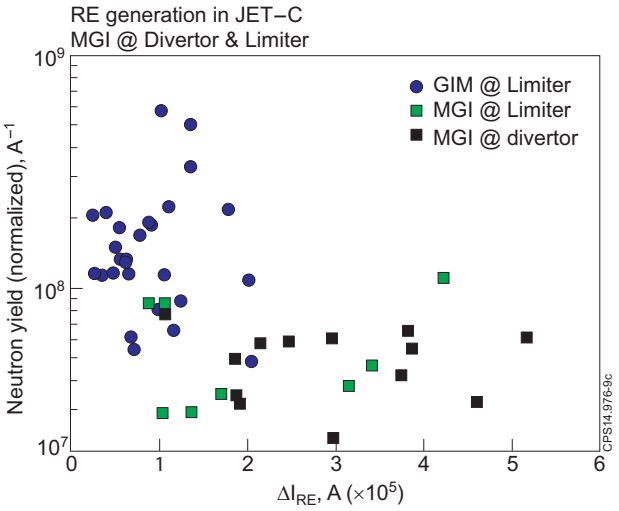

Figure 9: Normalized neutron yield versus lost RE current fractions in JET-C. Comparison of MGI and GIM injection effects on energetic characteristics of RE.

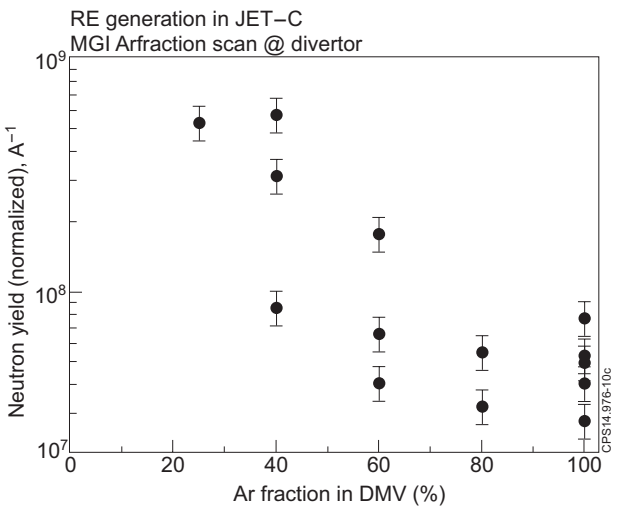

Figure 10: Dependence of normalized photoneutron yield versus Ar fraction in MGI at divertor configuration in JET-ILW.